Chapter 2

CALCITE DISSOLUTION RATES IN SEAWATER: LAB VS. IN-SITU MEASUREMENTS AND INHIBITION BY ORGANIC MATTER

2.1 Introduction

Ever since the first *in-situ* measurements of marine carbonate dissolution provided evidence for a non-linear rate response to undersaturation (Berger, 1967; Peterson, 1966), extensive work has been dedicated to untangling the relationship between dissolution rate and Ω. In the absence of a mechanistic understanding of the reactions in seawater, the oceanographic community has historically fit dissolution rates to an empirical equation of the form (Morse et al., 2007; Morse and Arvidson, 2002):

$$R_{diss} = k(1 - \Omega)^n \quad (1)$$

Here, k is the rate constant (mol cm^{-2} s^{-1}), Ω is a measure of the thermodynamic driving force, and n is the pseudo reaction order. Dissolution in low ionic strength aqueous solutions can be adequately described by Eq. (1) with n = 1 (Arakaki and Mucci, 1995; Cubillas et al., 2005; Svensson and Dreybrodt, 1992), as can the dissolution of packed calcite beds (Boudreau, 2013; Sulpis et al., 2017), but the dissolution of suspended calcite powder in seawater requires a non-linear reaction order ranging from 3-4.5 (Dong et al., 2018; Keir, 1980; Morse, 1978; Morse and Berner, 1972; Naviaux et al., 2019b; Subhas et al., 2015, 2017; Walter and Morse, 1985).

The non-linearity of Eq. (1) in seawater is consistent with the calcite surface transitioning through three dissolution mechanisms that become active at different critical saturations ("$\Omega_{critical}$s"): retreat of pre-existing steps for Ω = 1 to $\Omega_{critical} \approx 0.9$, the opening of etch pits at defects for Ω ≈ 0.9 to $\Omega_{critical} \approx 0.75$, and the opening of etch pits homogenously across the surface for Ω < 0.75 (Naviaux et al., 2019b). These surface processes have been previously identified in studies of calcite dissolution in low ionic strength aqueous solutions (Teng,

2004; Xu et al., 2012), but the $\Omega_{critical}$s for the activation of each mechanism occur significantly closer to equilibrium in seawater (Naviaux et al., 2019b). In this mechanistic framework, dissolution rates set by etch pit formation (R_{2D}), either at defects or homogenously across the surface, can be fit by (Dove et al., 2005):

$$\ln\left(\frac{R_{2D}}{(1-\Omega)^{\frac{2}{3}}|\sigma|^{\frac{1}{6}}}\right) = \ln\left(h\beta C_e(\omega^2 h n_s a)^{\frac{1}{3}}\right) - \frac{\pi\alpha^2\omega h}{3(k_b T)^2}\left|\frac{1}{\sigma}\right| \quad (2a)$$

Here, the left hand term is the normalized dissolution velocity (m s^{-1}), $|\sigma|=\ln(\Omega)$ is a measure of the solution driving force, h is the step height (m), β is the rate constant for surface retreat (step kinetic coefficient, m s^{-1}), ω is the molecular volume (m^3), n_s is the density of active nucleation sites (sites m^{-2}), a is the lattice spacing (m), α is the step edge free energy (J m^{-2}), k_b is Boltzmann's constant (J K^{-1}), T is the temperature (K), and C_e is the mineral solubility (atoms m^{-3}). Eq. (2a) describes a straight line with a slope set by a single term (the step edge free energy, α), and an intercept set collectively by the step kinetic coefficient (β) and the number of active nucleation sites (n_s). All other terms are either fundamental mineral properties assumed to be constant (h, ω, a), or are determined by the experimental conditions (C_e, T, Ω, σ).

Dissolution by the retreat of pre-existing steps and screw dislocations (R_{step}) dominates near equilibrium and is described by an equation that is non-linear with respect to $\left|\frac{1}{\sigma}\right|$:

$$\ln\left(\frac{R_{step}}{(1-\Omega)^{\frac{2}{3}}|\sigma|^{\frac{1}{6}}}\right) = \ln\left(\frac{\omega\beta C_e m h}{P}\right) + \ln\left((1-\Omega)^{\frac{1}{3}}\left|\frac{1}{\sigma}\right|^{\frac{1}{6}}\right) - \ln\left(1+8\left(\frac{\omega\alpha}{P k_b T}\right)\left|\frac{1}{\sigma}\right|\right) \quad (2b)$$

Here, the added terms are the number of elementary steps (m, order 1), and the perimeter of the screw dislocation core sourcing the steps (P, proportional to $2\pi mh$).

The work of Naviaux et al. (2019) more generally shows that n and k are variable functions of Ω and temperature, so attempts to describe marine calcite dissolution rates with a single fit to Eq. (1) will fail. The $\Omega_{critical}$s associated with each mechanistic transition are also temperature dependent, with the transition from step retreat to defect assisted etch pit formation being suppressed at 5°C. In other words, at the temperatures most relevant to undersaturated ocean waters, dissolution exhibits a weak dependence on Ω when $0.75 < \Omega < 1$ ($n < 1$) until the activation of homogenous etch pit formation at $\Omega_{critical} \approx 0.75$. Since each mechanistic regime responds differently to changing environmental variables, dissolution rates from one saturation range cannot be extrapolated to others.

Several fundamental issues remain to be solved in the field of seawater calcite dissolution kinetics, one of which is that dissolution rates measured in the lab (Keir, 1980; Morse, 1978; Morse and Berner, 1972) are consistently faster than those measured *in-situ* (Berelson et al., 1994; Berger, 1967; Fukuhara et al., 2008; Honjo and Erez, 1978; Milliman, 1975; Peterson, 1966). Some of the discrepancy results from comparisons between minerals of different size fractions (Morse, 1978) and dissolution histories (Arvidson et al., 2003; Arvidson and Luttge, 2010; Fischer et al., 2014, 2012), but the remaining offset is generally explained by the presence of inhibitors in natural seawater.

The most commonly invoked inhibitors are soluble reactive phosphate (SRP) and dissolved organic carbon (DOC). Both SRP and DOC adsorb to the calcite surface (de Kanel and Morse, 1978; Millero et al., 2001; Suess, 1973; Zullig and Morse, 1988) and have been shown to affect rates of calcite dissolution (Alkattan et al., 2002; Barwise et al., 1990; Berner et al., 1978; Berner and Morse, 1974; Compton et al., 1989; Compton and Sanders, 1993; Oelkers et al., 2011; Sjöberg, 1978; Thomas et al., 1993) and precipitation (Berner et al., 1978; Burton and Walter, 1990; Dove and Hochella, 1993; Hoch et al., 2000; Inskeep and Bloom, 1986; Kitano and Hood, 1965; Lin et al., 2005; Mucci, 1986; Reddy, 1977; Reynolds, 1978; Zullig and Morse, 1988). The magnitude of the effects vary greatly between studies,

and some carried out in seawater reported little influence of SRP (Walter and Burton, 1986) and DOC (Morse, 1974; Sjöberg, 1978) on calcite dissolution kinetics. These contrasting results warrant further study, and the finding that the calcite dissolution mechanism varies with Ω and temperature (Naviaux et al., 2019b) means that inhibitor effects should be explicitly investigated near equilibrium.

Another fundamental issue facing the oceanographic community is that individual measurements of the seawater CO_2 system parameters yield internally inconsistent values (Carter et al., 2018, 2013; Fong and Dickson, 2019; McElligott et al., 1998; Patsavas et al., 2015; Raimondi et al., 2019; Williams et al., 2017). Advances in measurement techniques (Dickson, 1993; Liu et al., 2011) have revealed that pH on the total hydrogen ion scale (pH_T) measured spectrophotometrically is offset from pH_T calculated from combinations of alkalinity (Alk), total dissolved inorganic carbon (DIC), and/or pCO_2. The discrepancy between measured and calculated pHs is itself pH dependent (Carter et al., 2018), so the offset cannot be explained simply by the inherent uncertainty in the seawater CO_2 system parameters (Orr et al., 2018). Whereas internal consistency between measurements and calculations can, in some cases, be attained by accounting for excess "organic alkalinity" (Cai et al., 1998; Patsavas et al., 2015; Yang et al., 2015) and adjusting the carbonic acid dissociation constants and the total boron-salinity ratio (Fong and Dickson, 2019), these adjustments are currently empirical. Hence, a more accurate description of seawater CO_2 chemistry is critical for our understanding of marine carbonate dissolution. For example, the position of the $\Omega = 1$ saturation horizon, defined as the depth in the water column below which calcium carbonate minerals should begin to dissolve, shifts by up to ~10% depending on the choice of parameters used to calculate Ω (Patsavas et al., 2015). Without a way to evaluate the "true" *in-situ* Ω, the position of the "true" saturation horizon remains unknown (Carter et al., 2018)

In this study, we attempt to reconcile and explain the long-standing discrepancies between calcite dissolution rates measured in the lab and in the field, as well as investigate how to best evaluate the "true" saturation horizon. We use a newly developed *in-situ* reactor to

quantify dissolution rates of ^{13}C-labeled inorganic calcite across an August 2017 transect of the North Pacific Ocean on the Calcite Dissolution Kinetics-IV (CDisK-IV) field campaign, and we compare these *in-situ* rates to rates measured under laboratory conditions. We use a surface energetic framework (Dove et al., 2005; Naviaux et al., 2019b) to demonstrate that the same dissolution mechanisms occur in the field as they do in the lab. We investigate the effects of several different natural inhibitors, and we demonstrate that our results may be used to describe previous *in-situ* inorganic calcite dissolution measurements.

2.2 Methods

2.2.1 Description of Materials

This manuscript focuses on the dissolution of ^{13}C calcite, but the *in-situ* reactor was tested prior to deployment using both ^{13}C calcite and ^{13}C-labeled coccolithophores (Subhas et al., 2018). Isotopically pure ^{13}C calcite was purchased from Sigma Aldrich (SKU 492027, > 99 atom%) and wet-sieved with 18.2 MΩ cm^{-1} water into 70-100 and 20-53 μm size fractions, the specific surface areas of which were determined by Kr-gas BET to be 0.09 ± 0.004 m^2 g^{-1} and 0.152 ± 0.006 m^2 g^{-1}, respectively (Naviaux et al., 2019b; Subhas et al., 2015). Laboratory measurements of calcite dissolution (protocol in Section 2.2.2) were carried out using both size fractions, and the dissolution rates agreed within experimental reproducibility (10% for dissolution rates of 10^{-15} – 10^{-10} mol cm^{-2} s^{-1}) once normalized to their respective surface areas (Naviaux et al., 2019). A more detailed discussion of the rinsing and surface area normalization procedures may be found in Naviaux et al. (2019). *In-situ* ^{13}C calcite dissolution measurements were carried out using only the 20-53 μm size fraction.

Coccolithophores (*E. huxleyi*) were cultured in ^{13}C-labeled seawater and were determined to have a specific surface area of 10.4 m^2 g^{-1} using Kr-gas BET (Subhas et al., 2018). A detailed description of the culturing and harvesting procedures may be found in Subhas et al. (2018). Subhas et al. measured the dissolution rates of both bleached and unbleached coccoliths, but only the bleached samples were used in the preliminary tests of the *in-situ* dissolution reactor.

2.2.2 Laboratory Measurements of Dissolution

Pure ^{13}C calcite and ^{13}C-labeled coccolithophores were dissolved under conditions of near constant alkalinity, DIC, Ω, and mineral surface area according to previously published methods (Naviaux et al., 2019b; Subhas et al., 2018, 2015, 2017). Briefly, 1-5 mg of pre-weighed, labeled material was placed within gas-impermeable Supelco bags (Sigma Aldrich: part no. 30336-U) that had been modified to include a custom sampling port with built-in filter. The bags were subsequently heat-sealed, evacuated of headspace, and filled with ~300g of seawater (seawater sourcing discussed below) of known alkalinity and DIC. The alkalinity of the seawater, and therefore its saturation state, was adjusted via titration with 0.1M HCl prior to filling the experimental bags. After filling, bags were placed in a water bath at 5 or 21°C and mounted on a shaker table set to 85 rpm. This shake rate has been shown to avoid diffusion limitation of the dissolution rate (Dong et al., 2018; Naviaux et al., 2019b; Subhas et al., 2015). Samples were withdrawn every six to twelve hours and measured simultaneously for DIC (± 2-4 μmol kg^{-1}) and $\delta^{13}C$ of the DIC ($\delta^{13}C$-DIC, ± 0.02‰) on a modified Picarro cavity ringdown spectrometer (Subhas et al., 2015). Alkalinity (± 1-3 μmol kg^{-1}) was measured potentiometrically at the beginning and end of each experiment via open-system Gran titration end-point determination (Dickson, 2007). Typical experiments dissolved < 10^{-7} moles of calcite, so alkalinity, DIC, and mineral surface area remained constant within measurement uncertainty. The $\delta^{13}C$ measurements at each timepoint were converted to number of moles dissolved, and the overall dissolution rate was determined from a linear fit to data collected after 24 hours. The initial non-linear equilibration period is well understood and is a result of simultaneous gross dissolution and precipitation fluxes coming into steady state (Subhas et al., 2017).

Laboratory saturation states were calculated using alkalinity-DIC pairs as input parameters in CO2SYS v1.1 (van Heuven et al., 2011) with the carbonic acid system K_1' and K_2' dissociation constants from the Lueker et al. (2000) refit to Mehrbach et al.'s (1973) data, calcite K_{sp}' from Mucci (1983), K_{HSO4} from Dickson (1990a), and K_{boron} from Dickson (1990). The total boron-salinity ratio was taken from Lee et al., (2010). The standard errors in DIC and alkalinity were propagated using a Monte Carlo approach (Subhas et al., 2015),

yielding final errors on Ω of 0.01-0.04 units. One of the goals of our research was to evaluate the offset between Ω calculated from alkalinity and DIC ($\Omega_{(Alk,\ DIC)}$), and Ω calculated from alkalinity and pH ($\Omega_{(Alk,\ pH)}$). Since the offset is systematic rather than random, the Ω errors we report are a description of our measurement precision, and do not include the uncertainty in the carbonic acid system dissociation constants (Orr et al., 2018).

Dissolution experiments were conducted in either Dickson Seawater Reference Material (Dickson, 2010) or archived seawater collected from the North Pacific during the CDisK-IV field campaign in August 2017. Dickson seawater was acquired from the Scripps Institution of Oceanography of the University of California, San Diego, where it was sterilized via UV-treatment, 0.2 μm filtration, and poisoned with $HgCl_2$. The practical salinity of the batches used ranged from 33.2 to 33.6, and the SRP and dissolved nitrate concentrations were between 0.3-0.5 and 0.36-5.1 μmol kg^{-1}, respectively. North Pacific seawater was collected from a CTD (conductivity, temperature, depth) cast from a depth of 75 m at 35°16.346 N, 150°59.515 W (Station 3), where it was immediately transferred into a 10L carboy and poisoned with $HgCl_2$ to a concentration of 0.0015% by weight. The archived water had a practical salinity of 33.905, SRP concentration of 0.293 μmol kg^{-1}, dissolved nitrate concentration of 2.07 μmol kg^{-1}, and was not filtered. The water was transferred into gas impermeable bags upon arrival on shore in September 2017, and dissolution experiments were conducted the following month.

Inhibition experiments were conducted by adding different compounds to Dickson seawater and evaluating the resulting change in calcite dissolution rates. Due to the varied and contradictory reports of the effects of SRP and DOC, experiments were designed to establish an upper limit to the inhibitory response that could be expected in open ocean environments. DOC in the upper water column is composed of, among other things, a complex array of mono and dicarboxylic acids (Moran et al., 2016). Gallic (CAS: 149-91-7) and oxalic acid (CAS: 133-62-7) were initially selected as model compounds to represent marine DOC. The effect of D-(+)-glucose (CAS: 50-99-7) was later investigated after it was noted that respiration in our archived seawater increased the DIC without a corresponding increase in

alkalinity (Section 2.3.3). Concentrated stock solutions of gallic acid, oxalic acid, KH_2PO_4 (CAS: 7778-77-0), and D-(+)-glucose were each prepared in 18.2 MΩ cm^{-1} water that had been adjusted to an ionic strength of 0.5M using NaCl. To eliminate variability in inhibitor concentrations between replicate experiments, ~1 mL of stock solution was injected into a 3 L reservoir of Dickson seawater before being divided into smaller batches for use in dissolution experiments. Final concentrations were 100 µmol kg^{-1} (glucose) or 20 µmol kg^{-1} (all other compounds).

2.2.3 *In-situ* Reactor Design and Lab Verification

Sixteen 1.7L Niskin bottles (General Oceanics SKU 101001.7) were modified to include a recirculating pump system that would allow ^{13}C labeled coccoliths, aragonite (Dong et al., 2019), and calcite to dissolve without diffusion limitation (Figure **2.1**). Once closed at depth, water sealed within the reactor flows over the material and accumulates ^{13}C-DIC from dissolution. The difference between the $\delta^{13}C$-DIC in the reactor bottle and that of the surrounding water column is a direct measure of the amount of dissolution that occurred, and dividing by the deployment time provides a rate.

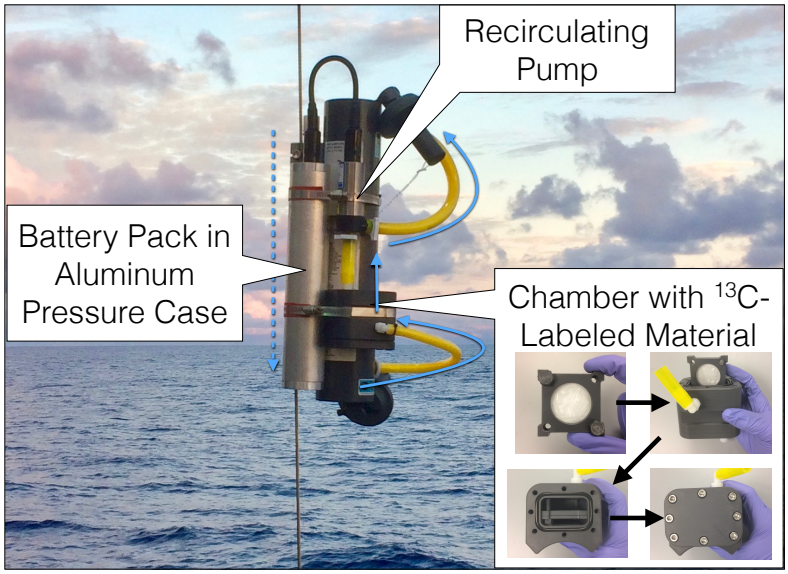

Figure 2.1: A standard 1.7L Niskin bottle was modified for dissolution experiments. A chamber containing ^{13}C-labeled material sealed within mesh packets was affixed to the

side, along with a recirculating pump and an aluminum pressure case to hold the batteries. The pump operates continuously and pushes water over the labeled material in the direction of the blue arrows.

To create the recirculating system, the bottom port of each Niskin was connected, using MasterFlex tubing (Tygon Fuel & Lubricant Tubing, 06401-82 and 06401-17), to a custom side chamber where labeled material could be easily accessed and exchanged between deployments. Additional tubing connected the top of the chamber to the inlet of a pump (Seabird SBE 5M mini pump, part 05M.2120), the outlet of which was routed to the top Niskin port by a final section of tubing. The pump drew water from the bottom of the Niskin to the top at a rate of 5 mL s^{-1} and was powered by four 1.5 V D-cell batteries held in an aluminum pressure case. A plastic insert was epoxied (DevCon 2 Ton Epoxy) inside each Niskin to decrease its internal volume and therefore enhance dissolution signals. The powder chamber had an internal volume of 300 ml, and the volume of all components totaled 1.1 liters. Given the flow rate of the pump, water recirculated within the reactor every four minutes, and the residence time of water in the powder chamber was just one minute.

Labeled material was pre-weighed and heat-sealed into packets of 47 mm diameter “Nuclepore” polycarbonate filters (Sigma Aldrich SKU: WHA111116) with pore sizes of 0.8 μm (coccoliths) or 8 μm (calcite) using a Safstar 12" Manual Impulse Heat Sealer (Amazon.com ASIN: B06X6MTLY3). Coccolith and calcite packets contained 0.5-1.5 mg and 10-12 mg of material, respectively. Calcite packets were subdivided in halves with ~5 mg of powder each to prevent clumping. Packets were pressed between two custom plastic mounts to ensure that they remained in the flow path of the water and did not clog the chamber inlet or outlet. The mounts had an open face diameter of 45 mm on each side and were held together by plastic screws at their corners. Up to two mounts could be placed within the reactor side chamber at once. An o-ring was placed in a groove at the top of the chamber and greased with Dow Corning Vacuum Lubricant (Amazon.com ASIN: B001UHMNW0) before bolting on a sealing plate.

The modified reactors were tested before deployment to ensure that they reproduced dissolution rates measured in calcite (Naviaux et al., 2019b) and coccolith (Subhas et al., 2018) benchtop experiments. One of the first issues that was investigated was the effect, if any, of sealing labeled material within Nuclepore packets. Benchtop experiments were conducted following the same methods as outlined above, but material was sealed in 0.8 µm (coccoliths) or 8.0 µm (calcite) Nuclepore packets rather than being dispersed as free powder within the Supelco bag. Dissolution rates of all materials within Nuclepore packets matched those derived from dispersed powder, but the δ^{13}C-DIC signals differed in how they evolved over time (Figure **2.2** inset). Whereas dispersed powder experiments display a period of initial curvature before becoming linear (Subhas et al., 2017), the Nuclepore packets produce a linear dissolution signal over the entire experimental period. The linear signal served to our advantage in the field, as it meant that dissolution rates could be determined from a two-point calculation, regardless of the reaction time.

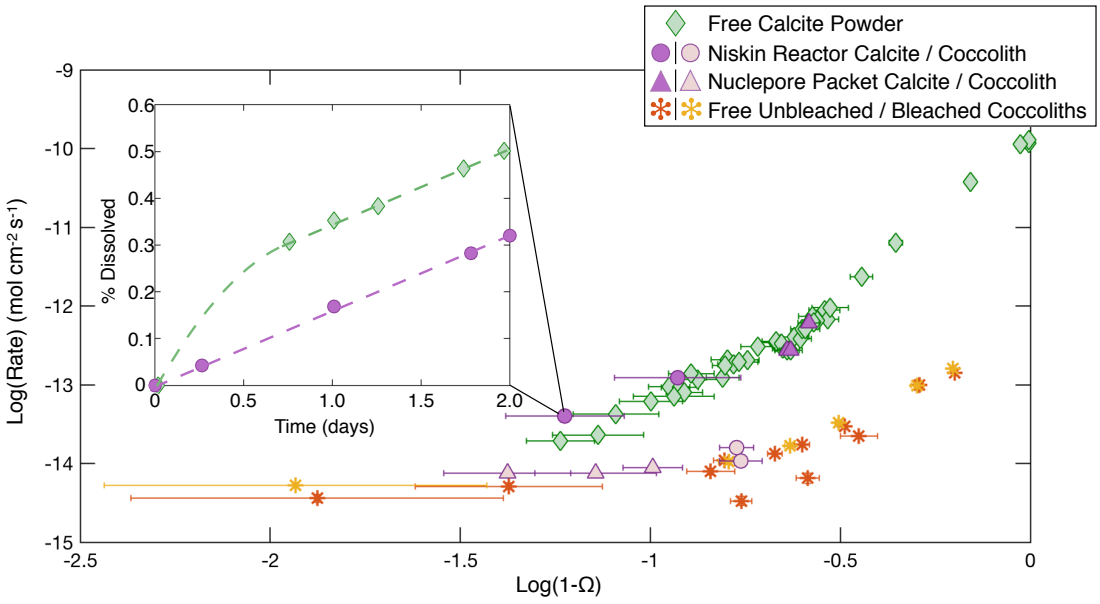

Figure 2.2: The dissolution rates of labeled material at 21°C in Nuclepore mesh packets (triangles) and fully assembled Niskin reactors (circles) agree with dissolution rates of dispersed calcite (diamonds) and coccoliths (stars) in Supelco bags. Rate errors are smaller than the symbols. Inset: The time evolution of the δ^{13}C signal (normalized by percent of

total mass dissolved for comparison) for dispersed powder and powder in Niskin reactors with dashed lines to guide the eye.

We applied the box model of Subhas et al. (2017) to our Nuclepore packet data to understand the linearization of the δ^{13}C-DIC versus time signal. The box model describes calcite dissolution rates using three main reservoirs: a reactive calcite layer, a diffusive boundary layer, and the bulk solution. Simultaneous dissolution and precipitation reactions occur between the reactive layer and the boundary layer, and the balance of fluxes sets the net dissolution rate. The δ^{13}C of DIC is calculated within each reservoir at every timestep. A complete description of the model may be found in the supplement to Subhas et al. (2017). We found that the signal linearization we observed could be explained by an increase in total boundary layer volume from ~1.3 µL to ~1.3 mL. This increase agrees with the approximate volume of each Nuclepore packet. As expected, a further increase of the boundary layer thickness would eventually lead to dissolution inhibition (Figure **2.3**).

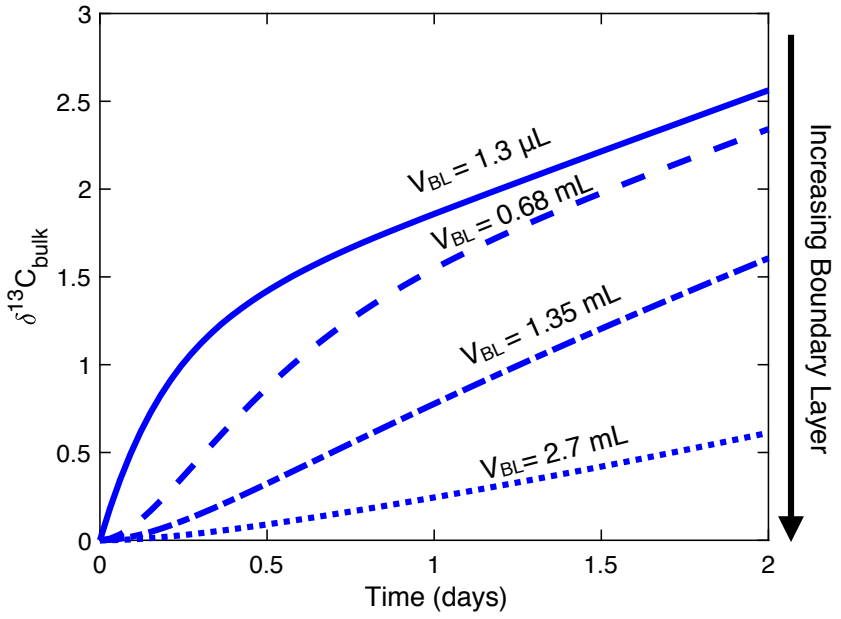

Figure 2.3: Example outputs from the model of Subhas et al. (2017) demonstrating that increased boundary layer volumes (V_{BL}) can cause dissolution signals to appear linear while expressing the same net rate (top three fits) Continuing to increase the boundary layer

eventually inhibits dissolution (bottom fit). These outputs were generated using: R_{Diss} = $5 \cdot 10^{-13}$ moles s^{-1}, R_{Diss}/R_{Precip} =1.12, Mass = 1.5 mg $CaCO_3$, Surface Area (SA)= 900 cm^2 g^{-1}, and varying boundary layer thickness (BL_T) from 10 μm to 20 mm to achieve the desired $V_{BL} = BL_T \cdot SA \cdot Mass$

Having demonstrated that Nuclepore packets themselves did not affect the net reaction rate in the range of saturations expected at sea, we assembled a prototype system with which to test how the packets performed in the *in-situ* reactor. Packets containing 1 mg or 10 mg (coccoliths, calcite) of material were loaded into the reactor side chamber before filling the reactor with 0.2 μm-filtered, $HgCl_2$-poisoned seawater collected off the coast of Catalina Island. Reactors were closed and submerged in a large water bath, at which point the experiment was considered started. Each reactor was sampled regularly over the course of two days for DIC, alkalinity, and δ^{13}C-DIC. Similar to their benchtop counterparts, no change in the alkalinity or DIC of the system was observed, and dissolution rates of both calcite and coccoliths agreed between all methods (Figure **2.2**).

2.2.4 Deployment of Reactors in the Field

In-situ dissolution rates were measured at four of five stations along a transect in the North Pacific from Honolulu, Hawaii to Seward, Alaska. Conductivity, temperature, depth (CTD) casts were taken prior to reactor deployments to determine the background profiles of salinity, temperature, silica, total DIC, alkalinity, pH, and δ^{13}C-DIC. Niskin reactors were attached to the hydrowire and lowered to the desired depths (as determined by the measured background Ω profile) and triggered shut. Another set of *in-situ* reactors was fixed to a weighted wire line, triggered shut at depth, and subsequently attached to surface floats and set free drifting from the ship. Reactor pumps operated continuously and served to flush the bottles with seawater and pre-rinse the labeled material as the Niskins descended through the water column. The Niskin reactors remained closed at depth for 24-58 hours and were sampled for silica, SRP, nitrate, alkalinity, pH, and δ^{13}C-DIC upon recovery. Samples were collected within three minutes of opening the Niskin and were drawn from the bottom port to minimize DIC exchange with ambient air.

2.2.5 Field Sampling Methods

The entire volume of each reactor was utilized for sample analysis. Four 10 ml samples were withdrawn and injected through a 0.2 μm syringe filter into evacuated exetainer vials for δ^{13}C-DIC measurements on a Picarro CRDS. Samples were standardized against pre-weighed amounts of solid ^{13}C-calcite to correct for signal drift over time. The standard deviation on sample replicates was ±0.05‰. The dissolution rate error was calculated from the relative error of the measurement divided by the change in δ^{13}C-DIC signal in the bottle compared to the background water column. Given the precision of the Picarro and the size of the signals, rate errors were typically below 5%. Nevertheless, rate errors could exceed 50% near equilibrium ($0.85 < \Omega < 1$) when dissolution signals were only 0.2-0.3‰ above background.

Immediately following δ^{13}C-DIC sampling, the Byrne group from the University of South Florida withdrew samples for pH and alkalinity measurements. Including the rinsewater, a total of 100 mL were used for pH measurements, and 600 mL for alkalinity. pH_T was spectroscopically measured to a precision of ± 0.001 units using a purified meta-Cresol Purple (mCP) dye indicator according to previously published methods (Liu et al., 2011). Alkalinity was measured following weak acid additions to a precision of ± 3 μmol kg^{-1} using a bromocresol purple dye indicator (Liu et al., 2015). Silica samples were subsequently taken and measured to ± 1.5 μmol L^{-1} using the standard molybdate reduction method (Mullin and Riley, 1955; Parsons, 2013). The remaining liquid was filtered (0.2 μm) into 15 mL Falcon tubes, refrigerated, and stored. These archived samples were sent immediately following the cruise in a cooler with Blue Ice to the University of Maryland for analysis of dissolved nitrate (± 0.25 μmol L^{-1}) and soluble reactive phosphate (± 0.03 μmol L^{-1}) concentrations.

Saturation states in the Niskin reactors were determined from Alk-pH pairs due to sample volume restrictions, rather than from Alk-DIC pairs as was done for laboratory experiments. The difference between the Ω calculated from these pairs will be discussed in greater detail in Section 2.3.1. Alkalinity and pH_T measurements were input into CO2SYS along with the temperature, salinity, depth, SRP, and silica concentrations at which the reactor was

deployed. The saturation state was calculated using the same acid dissociation constants and Monte Carlo error propagation procedure as in the lab, but the precision of the pH measurements meant that Ω was constrained to ± 0.005 units.

2.2.6 Quality Checking Reactors

Reactor failures were diagnosed by comparing the silica concentration in each reactor with that of the background profile as recovered from the CTD cast. Occasionally, bottles did not seal properly when closing and would mix in outside water as they were drawn up through the water column upon recovery. This artificially increased/decreased calculated dissolution rates as heavier/lighter δ^{13}C-DIC water infiltrated the bottle. Silica exhibits a large gradient with depth in the ocean, so leaks were clearly identified (Figure **2.4**) and dissolution data were discarded from any reactors whose silica concentrations deviated from background by more than 1 standard deviation (1.5 µmol L^{-1}).

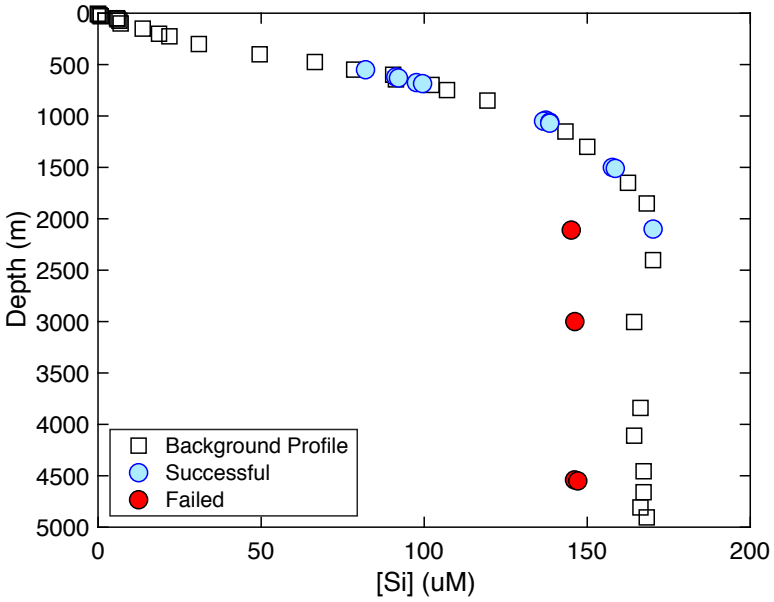

Figure 2.4: Example of how failed reactors were identified at Station 4. Background profiles of silica (squares) were determined prior to reactor deployment. Reactors were sampled for silica after recovery and were deemed successful (blue circles) if their measured silica concentration was within one standard deviation (± 1.5 µmol L^{-1}) of the

background profile. Data from failed reactors (red circles) were easily identified and subsequently discarded.

Miniature pressure/temperature loggers (Star-Oddi: model DST centi-TD) were mounted on each reactor to quantify variations in bottle depth resulting from ship heave and/or wire angle. If these changes were large, they would change the temperature and pressure experienced by the reactor, and therefore the calculated *in-situ* saturation state. Depth variations were on the order of 1-3 m and proved insignificant.

2.3 Results

2.3.1 Discrepancy in Ω Calculations

Consistent with previous reports (Carter et al., 2018, 2013; Fong and Dickson, 2019; McElligott et al., 1998; Patsavas et al., 2015; Raimondi et al., 2019; Williams et al., 2017), shipboard determinations of $\Omega_{(Alk, pH)}$s were systematically offset from $\Omega_{(Alk, DIC)}$s by ~5-10% (Figure **2**.**5**a-d). The shift in the saturation horizon ($\Omega = 1$) exceeded the measurement error at Stations 3, 4, and 5. Given that the CDisK-IV route was similar to the P16 North line from the World Ocean Circulation Experiment (WOCE), we compared our $\Omega_{(Alk, pH)}$ measurements with those from a P16 line conducted in 2015 (EXPOCODE: 33RO20150525) that measured pH spectrophotometrically to ensure that there was not a systematic error in our data. These data exhibit the same offsets as our own (Figure **2**.**6**a). Depth and pH_T are correlated, so the offset between measured and calculated pH increases from near zero at the surface to a maximum around 700-1000m. The offset then decreases deeper in the water column (Figure **2**.**6**b).

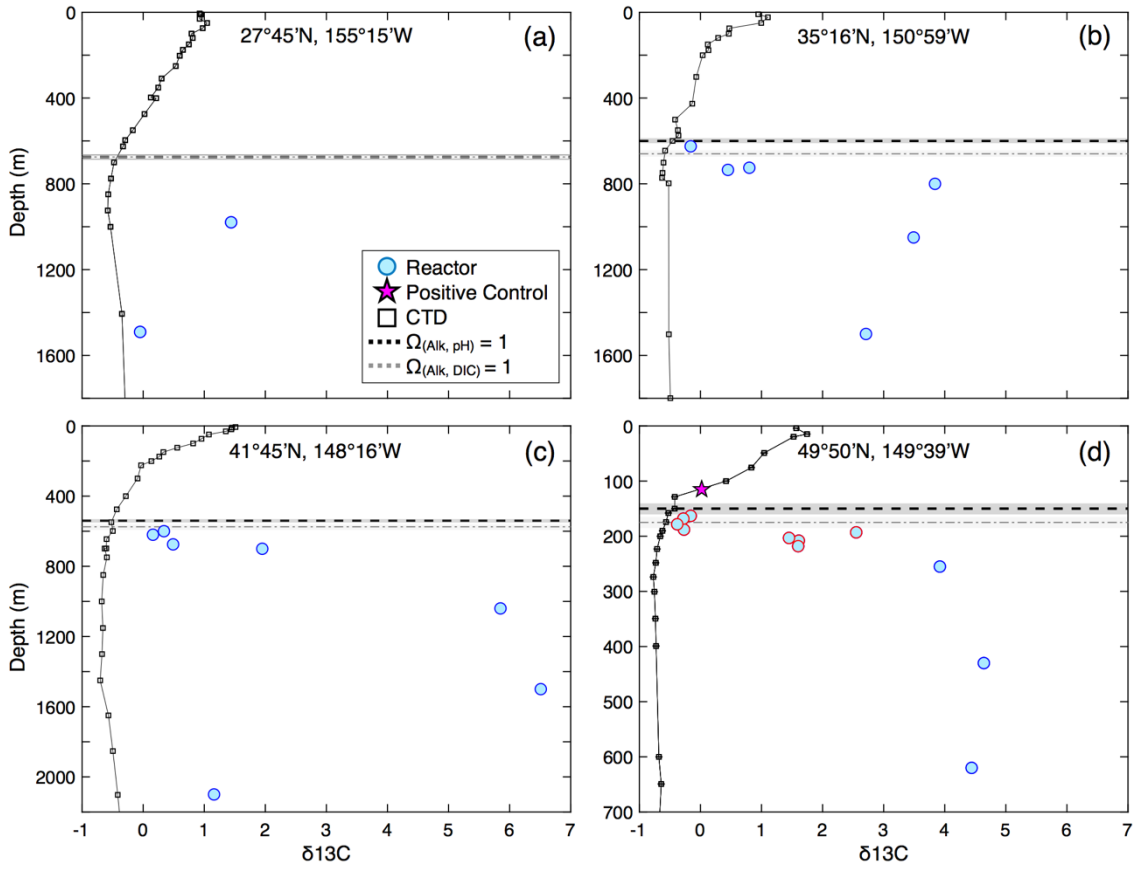

Figure 2.5: Background profiles of $\delta^{13}C$ (squares) measured at (a) Station 2, (b) Station 3, (c) Station 4, (d) Station 5, each plotted with the $\delta^{13}C$ measured in the Niskin reactors upon recovery (circles). Station 5 points outlined in red were deployed after a storm (see text for details). Errors on $\delta^{13}C$ measurements are smaller than the points. The dashed horizontal lines show $\Omega_{(Alk,\ pH)} = 1$ (black) and $\Omega_{(Alk,\ DIC)} = 1$ (grey) with corresponding uncertainty. The offset between $\Omega_{(Alk,\ pH)}$ and $\Omega_{(Alk,\ DIC)}$ exceeded measurement error at Stations 3, 4, and 5. Dissolution was observed when supersaturated for $\Omega_{(Alk,DIC)}$ but undersaturated for $\Omega_{(Alk,\ pH)}$ (b, d). No dissolution occurred when supersaturated for $\Omega_{(Alk,\ pH)}$ (star, d).

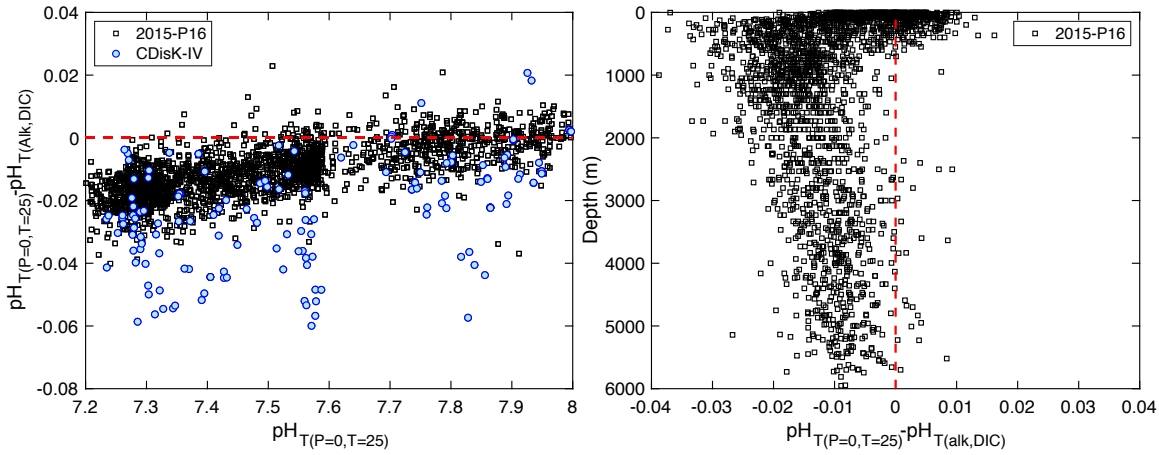

Figure 2.6: (a) The difference between measured pH_T and calculated $pH_{T(Alk, DIC)}$ versus measured pH_T for data collected on CDisK-IV and a 2015-P16 cruise. (b) 2015-P16 pH offsets versus depth.

Results from our dissolution reactors offer an independent verification of the Ω calculation that better describes seawater calcite chemistry. We deployed a reactor at Station 3 (151°W / 35.265°N) where waters were supersaturated according to our own measurements of Alk-DIC, but undersaturated according to Alk-pH. At a depth of 625m, we measured $\Omega_{(Alk, pH)} = 0.90 \pm 0.005$ and $\Omega_{(Alk, DIC)} = 1.07 \pm 0.06$. We observed an enrichment of 0.353‰ above the background profile of ^{13}C-DIC, whereas a positive control reactor deployed at $\Omega_{(Alk, pH)} = 1.29 \pm 0.005$ at Station 5 experienced no enrichment (Figure **2.5**a-3d). Consequently, we use $\Omega_{(Alk, pH)}$ for *in-situ* Ωs. The implications for historical $\Omega_{(Alk, DIC)}$s are discussed in Section 2.4.1.

No discrepancy between Ω calculations was observed when measuring Dickson seawater alkalinity, DIC, and pH under laboratory conditions. This could in part be due to the UV sterilization process destroying organic bases contributing to excess alkalinity, but this is an area for future study. We use uncorrected $\Omega_{(Alk, DIC)}$ for laboratory experiments.

2.3.2 *In-situ* Dissolution Results

Our *in-situ* measurements included 27 calcite reactors (Figure **2.5**a-d) deployed over depths, saturation states, and temperatures of 125-2100 m, Ω = 1.29-0.68, and 1.91-4.87°C, respectively; all of which passed the silica quality check criteria (Table 2.1). Dissolution Δ^{13}C-DIC signals of 0.20-7.18‰ were observed in undersaturated reactors, corresponding with dissolution rates of $1.63 \cdot 10^{-15}$ to $1.01 \cdot 10^{-13}$ mol cm^{-2} s^{-1}. No enrichment of δ^{13}C-DIC was seen in a positive control placed at Ω = 1.29, indicating that our signals represent true dissolution and are not a result of isotopic exchange. SRP and dissolved nitrate samples were collected from hydrocasts along the entire transect, as well as from 25 of the 27 Niskin reactors. Reactor nutrient concentrations varied from 2.1-3.3 μmol L^{-1} SRP and 29.8-46.7 μmol L^{-1} dissolved nitrate, with the lowest concentrations observed in the positive control reactor at 125 m.

Table 2.1: Results from *in-situ* Dissolution Reactors. Alkalinity and pH_T measured to ± 3 μmol kg^{-1} and ± 0.001 units, respectively, resulting in Ω ± 0.005 units

Station	Depth (m)	Alk (μmol kg^{-1})	$pH_{(P=0,T=25,S)}$	T (°C)	$\Omega_{(Alk, pH)}$	Practical Salinity	Phosphate (μm)	Nitrate (μm)	Silica (μM)	Powder Amount (mg)	$\delta^{13}C$ (‰)	Rate·10^{-15} (mol cm^{-2} s^{-1})	Rate error ·10^{-15} (mol cm^{-2} s^{-1})
2	979	2369	7.297	3.94	0.758	34.36	-	-	119.3	20.71	1.99	18.2	1.47
2	1491	2404	7.399	2.87	0.878	34.55	-	-	141.7	11.67	0.29	4.6	2.49
3	625	2306	7.343	4.87	0.897	34.04	2.61	39.91	83.7	21.41	0.36	2.6	1.17
3	725	2326	7.299	4.30	0.789	34.13	3.09	44.12	99.9	20.54	1.41	10.9	0.93
3	735	2327	7.294	4.25	0.777	34.14	3.03	43.05	100.8	10.82	1.07	15.8	1.76
3	800	2343	7.281	4.01	0.746	34.19	3.14	44.76	111.2	22.19	4.36	31.4	1.16
3	1050	2376	7.273	3.27	0.698	34.36	3.31	46.69	134.8	10.93	4.01	59.8	2.23
3	1500	2409	7.329	2.53	0.734	34.54	3.19	46.12	151.9	11.249	3.23	46.9	2.18
4	600	2313	7.335	4.46	0.885	34.06	2.74	41.98	87.3	21.9	0.84	7.9	1.70
4	700	2322	7.254	4.12	0.709	34.15	3.15	44.05	100.3	21.32	2.58	25.3	1.47
4	620	2318	7.323	4.37	0.858	34.08	2.88	40.84	91.3	21.65	0.70	4.8	1.10
4	675	2329	7.313	4.20	0.830	34.13	2.97	42.84	97.6	21.03	1.09	7.8	0.93
4	1040	2380	7.282	3.12	0.717	34.34	3.22	45.62	137.3	21.99	6.52	45.5	1.05
4	1500	2411	7.300	2.44	0.68	34.50	3.26	46.05	157.7	11	7.18	101.0	1.83
4	2100	2431	7.391	1.91	0.749	34.61	3.01	43.98	170.2	11.4	1.58	21.4	1.49
5	255	2293	7.241	3.77	0.745	33.85	2.94	43.12	88.2	21.78	4.65	19.8	0.68
5	430	2323	7.249	3.81	0.741	34.06	3.08	43.98	106.8	20.98	5.27	23.4	0.85
5	620	2347	7.267	3.57	0.750	34.21	3.14	44.26	120.0	21.47	5.05	22.2	0.48
5*	125	2246	7.462	3.95	1.287	33.19	2.11	29.77	47.4	21.21	0.00	0.0	-
						Post Storm Dissolution Measurements							
5	193	2278	7.273	3.68	0.736	33.76	2.86	41.48	78.5	22.02	3.18	25.8	1.21
5	208	2285	7.267	3.69	0.811	33.79	2.91	40.77	80.5	21.27	2.29	19.3	1.18
5	218	2295	7.275	3.71	0.801	33.81	2.89	41.69	82.1	20.79	2.30	19.9	1.29
5	203	2283	7.305	3.69	0.816	33.78	2.66	41.91	80.1	21.03	2.11	18.0	1.19
5	163	2277	7.285	3.64	0.883	33.70	2.75	39.7	71.0	23.23	0.38	2.9	1.28
5	188	2281	7.300	3.67	0.838	33.74	2.85	41.12	77.7	20.68	0.34	3.0	1.49
5	168	2277	7.281	3.65	0.872	33.70	2.71	39.84	74.3	23.17	0.27	2.1	1.14
5	178	2276	7.297	3.67	0.829	33.73	2.69	40.2	75.1	21.61	0.20	1.6	1.23

*Positive control

In-situ calcite dissolution rates exhibited a non-linear dependence on saturation state within the N. Pacific Ocean (Figure **2.7**). Dissolution rates increase gradually with undersaturation until Ω ≈ 0.75-0.80, after which calcite dissolves more rapidly in response to changes in Ω. This change in behavior is evident from the kink in the slope of the log-log plot near log(1-Ω) = -0.7 to -0.6 (Figure **2.7**b). Reactors deployed above the thermocline from 0 – 250 m showed greater rate variability than reactors at 250 – 2200 m. The variability in shallow reactors is related to whether they were deployed before or immediately after a storm that occurred at Station 5 (Figure **2.7** red outline). Whereas *in-situ* dissolution rates measured before the storm (diamonds at 1 - Ω = 0.25) followed the rate vs. Ω trend established at previous stations, data collected immediately following the storm (diamonds closer to equilibrium than 1 - Ω = 0.2) did not. The storm caused the water column temperature, salinity, as well as the oxygen and chlorophyll concentrations to all change dramatically. We hypothesize why the rate data are more scattered in Section 2.4.3.

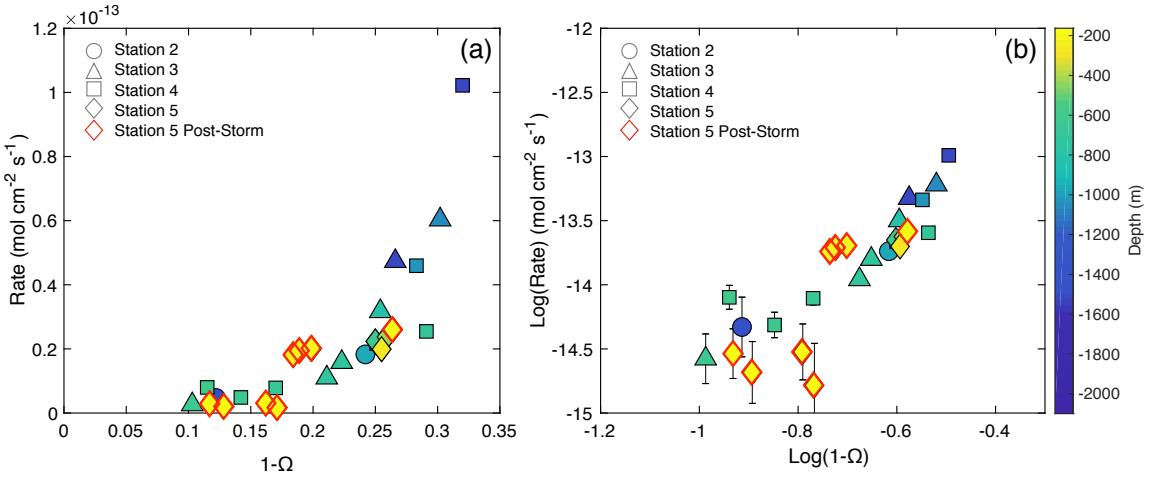

Figure 2.7: Dissolution rate (mol cm^{-2} s^{-1}) of synthetic calcite versus (a) 1-Ω and (b) Log(Rate) versus Log(1-Ω). Points are colored by their deployment depth, and reactors deployed after a storm at Station 5 are outlined in red. Error bars are plotted for both rate and Ω, but are frequently smaller than the symbols.

2.3.3 Laboratory Results

Dissolution rates measured in Dickson seawater at 5° C exhibit the same trends versus 1-Ω as documented *in-situ* (Figure **2**.**8**a), but rates measured in the laboratory are faster by a factor of ~4. No dissolution was observed in the lab at $\Omega = 1.05 \pm 0.02$ (not shown). Once undersaturated, 5°C laboratory dissolution rates increase from 0 to $\sim 1 \cdot 10^{-13.5}$ mol cm^{-2} s^{-1} by $\Omega = 0.99$ (Figure **2**.**9**) and remain nearly independent of Ω until $\Omega_{crit} \approx 0.8$. The offset between lab and *in-situ* rates is due to some difference in water chemistry that will be explored below, rather than a methodological bias, as experiments run soon after the cruise in archived N. Pacific seawater produced comparable rates as measured *in-situ* (Figure **2**.**8**b).

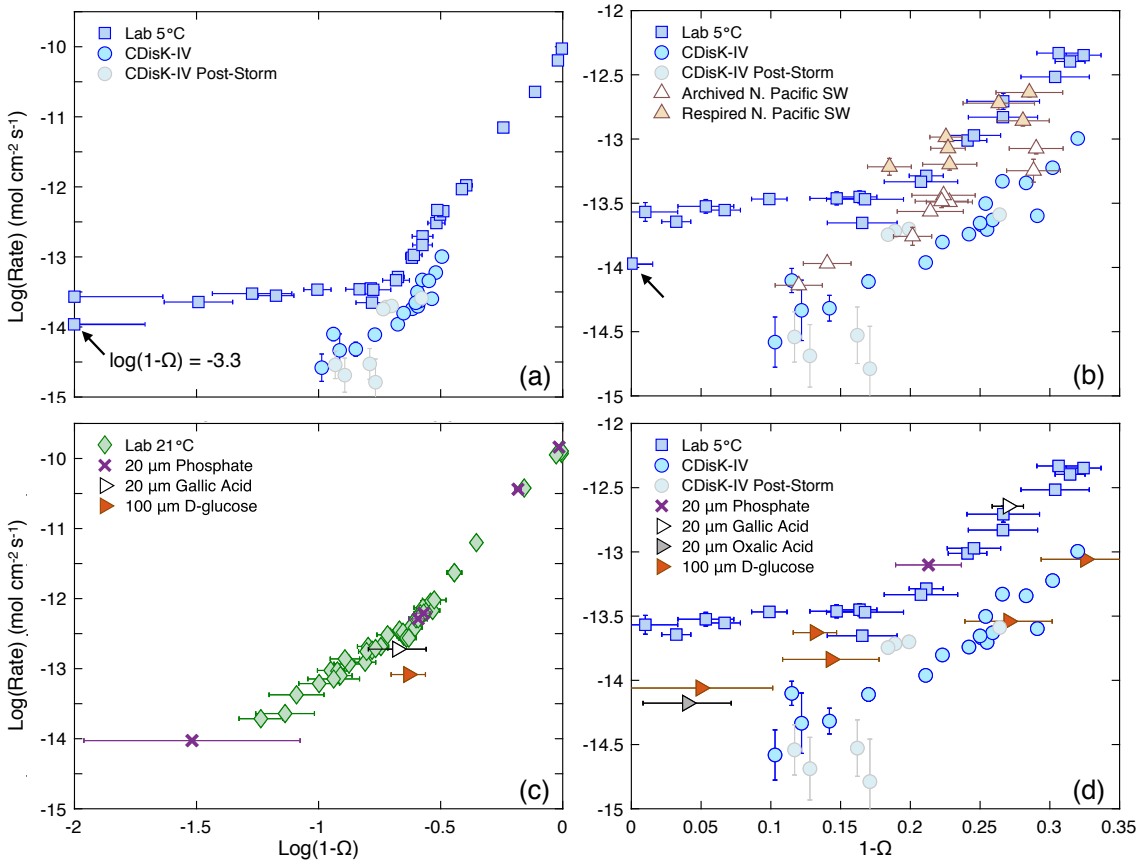

Figure 2.8: Comparisons of Log(Rate) (mol cm^{-2} s^{-1}) versus either Log(1-Ω) (a, c) or 1-Ω (b, d) for calcite dissolution experiments in the lab and *in-situ*. (a) Dissolution at 5°C in poisoned, filtered, UV-treated Dickson seawater (squares) versus dissolution measured *in-situ* in the N. Pacific (circles). The light grey circles are *in-situ* dissolution measurements made after the storm at Station 5. (b) Dissolution rates at 5°C in archived North Pacific seawater before (white triangles) and after (brown triangles) DIC increased by 152 µmol kg^{-1}. The arrow in (a) and (b) indicates a point at Log(1-Ω) = -3.3 which may be more clearly seen in the expanded version of this figure (Fig. S3). (c) Dissolution rates in Dickson seawater at 21°C (diamonds, from Naviaux et al. 2019) and with Dickson seawater spiked with different potential inhibitors. (d) The same as (c), but versus 1-Ω and with experiments conducted at 5°C. The point at Log(1-Ω) = -3.3 is left off of (d) for visual clarity.

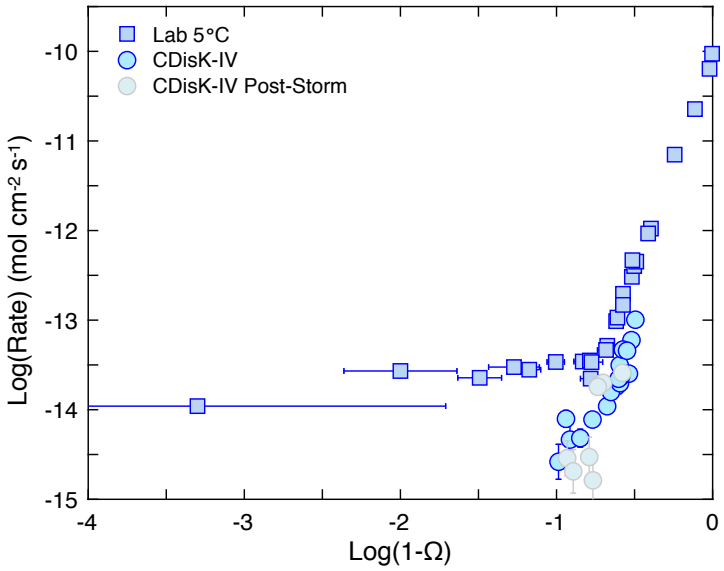

Figure 2.9: Expanded version of Figure 2.8a of Log(Rate) (mol cm^{-2} s^{-1}) versus Log(1-Ω) for calcite dissolution experiments in the lab and *in-situ*. No dissolution was observed at Ω = 1.05 ± 0.02 in the lab, but dissolution did occur at Log(1-Ω) = -3.3. The point at Log(1-Ω) = -3.3 is within error of Ω = 0, but still serves to demonstrate a slight Ω dependence for dissolution rates very near equilibrium.

Despite being stored in the dark in gas impermeable bags without headspace, the DIC of the archived seawater was found to have increased by 152 µmol kg^{-1} after 3 months. A leak in the bag would allow water to evaporate and alter both DIC and alkalinity, but the alkalinity of the water remained constant. No further change in water chemistry occurred over the following 6 months. Experiments conducted in the altered, archived seawater produced dissolution rates that matched the rates measured in Dickson seawater (Figure **2.8**b). We refer to this altered, archived seawater as "respired," and discuss our reasoning and the implications of the faster dissolution rate in Section 2.4.3.2.

Spiking Dickson seawater with different potential inhibitors had variable effects on dissolution, with the addition of 100 µmol kg^{-1} D-glucose slowing rates to comparable values as those measured in the N. Pacific (Figure **2.8**c, d). The degree of inhibition varied by compound, with temperature, and with distance from equilibrium. Glucose slowed calcite

dissolution rates by a factor of ~4 at 5 and 21°C for $\Omega < 0.8$, but had less of an effect closer to equilibrium. Gallic acid and orthophosphate had no effect on dissolution at either 5 or 21°C, but oxalic acid slowed rates near-equilibrium at 5°C by a factor of ~2. As discussed below, we attribute the variable effects of each compound to changes in dissolution mechanism across different saturation ranges.

2.4 Discussion

2.4.1 Implications for Ocean Saturation State

Our dissolution experiments suggest that $\Omega_{(alk,\ DIC)}$ calculations systematically overestimate *in-situ* calcite saturation. Three pieces of evidence indicate that the more undersaturated values for *in-situ* $\Omega_{(Alk,\ pH)}$ better capture marine calcite chemistry than $\Omega_{(Alk,\ DIC)}$: (1) At sea, carbonate dissolution was documented at Stations 3 and 5 in waters that were supersaturated for $\Omega_{(Alk,\ DIC),}$ but undersaturated for $\Omega_{(Alk,\ pH)}$. No dissolution occurred when waters were supersaturated by $\Omega_{(Alk,\ pH)}$. (2) *In-situ* dissolution exhibits a kink in rate at the same Ω_{crit} as in the lab, but only when comparing *in-situ* $\Omega_{(Alk,\ pH)}$ and lab $\Omega_{(Alk,\ DIC)}$. (3) Laboratory dissolution rates measured in archived N. Pacific seawater were comparably slow as those measured *in-situ*, despite using Alk-DIC pairs in the lab to place the rates in Ω space.

Until new values for the carbonic acid dissociation constants are experimentally verified or refined (Fong and Dickson, 2019), there will be systematic offsets between datasets depending on their choice of CO_2 chemistry input parameters. To illustrate this point, we plot the calcite Ω profiles at each of our stations in Figure **2.10** alongside $\Omega_{(Alk,\ pH)}$ from the 2015-P16 cruise, and $\Omega_{(Alk,\ DIC)}$ from the Global Data Analysis Project v2 (GLODAP, Olsen et al., 2016) database. The profiles of $\Omega_{(Alk,\ pH)}$ agree quite well with one another, but they are clearly offset from GLODAP $\Omega_{(Alk,\ DIC)}$. The discrepancy extends to abyssal waters, and therefore cannot be due to ocean acidification, which has only extended to intermediate waters in the Pacific (Byrne et al., 2010). Proxies thought to represent marine carbonate chemistry over glacial time periods, such as boron/calcium ratios, are frequently calibrated to GLODAP $\Omega_{(Alk,\ DIC)}$ (Yu and Elderfield, 2007). Whereas the uncertainties in the proxies themselves may be large, our *in-situ* dissolution results suggest a consistent offset in Ω

accuracy, rather than precision, with $\Omega_{(Alk, DIC)}$ being biased towards more saturated values. Caution should be used when applying such proxies until a thorough reevaluation of marine carbonate system parameters (Fong and Dickson, 2019) has been conducted.

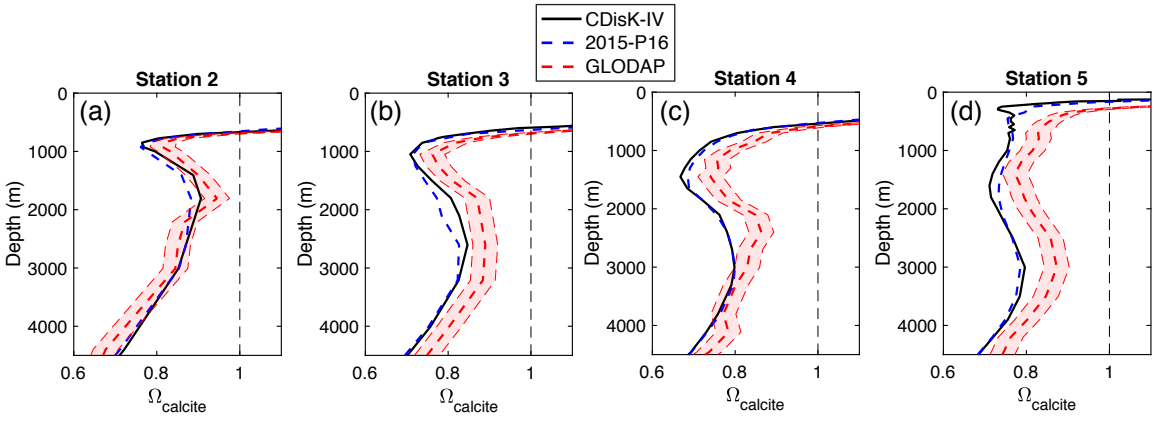

Figure 2.10: (a)-(d) Profiles showing the systematic offset between $\Omega_{(Alk, pH)}$ (from CDisK-IV and 2015-P16) and $\Omega_{(Alk, DIC)}$ (from GLODAP) at each station. The GLODAP profiles were derived from 2006-P16 cruise measurements (EXPOCODE: 325020060213) of Alk and DIC data flagged as "acceptable." Ω was calculated using the same CO_2 system parameters as discussed in the main text. GLODAP Alk and DIC were measured to better than ± 3 µmol kg^{-1}, corresponding with $\Omega_{(Alk, DIC)}$ ± 0.03. Measurement errors for $\Omega_{(Alk, pH)}$ are ± 0.005 and are not visible.

2.4.2 Laboratory versus *In-situ* Dissolution Rates

Dissolution in the lab and *in-situ* follow the same rate behavior versus undersaturation and undergo a change in surface mechanism at the same $\Omega_{critical}$ (Figure **2.11**a). Fits to the data are presented in Table 2.2. We use $\Omega_{critical} = 0.8$ rather than the 0.75 used previously (Naviaux et al., 2019b), as additional laboratory data collected at 5°C support a transition closer to equilibrium. The near-equilibrium fit to the *in-situ* data is constrained by only a few measurements, so the reaction order changes slightly depending on whether $\Omega_{critical} = 0.75$ or $\Omega_{critical} = 0.8$ is used. Nevertheless, this difference does not affect our overall analysis. In the traditional Rate = $k(1-\Omega)^n$ equation, dissolution in the lab and *in-situ* are both weakly dependent on undersaturation from $0.8 < \Omega < 1$, after which the reaction order increases to ~4.7. The log of the rate constant necessarily increases with n from -13.1 ± 0.2 to -10.0 ± 0.1

mol cm^{-2} s^{-1} for the 5°C lab data, and from -13.5 ± 0.4 to -10.8 ± 0.4 mol cm^{-2} s^{-1} for the *in-situ* data. We emphasize that the kink at $\Omega_{critical} \approx 0.8$ means that the use of a single *n* and *k* pair will systematically misfit dissolution rates.

Table 2.2: Fits to Empirical Rate Equation				
Condition	1 > Ω > 0.8		0.8 > Ω > 0	
	$Log_{10}k$ (mol cm^{-2} s^{-1})	*n*	$Log_{10}k$ (mol cm^{-2} s^{-1})	*n*
Laboratory 5°C	-13.1 ± 0.2	0.11 ± 0.1	-10.0 ± 0.1	4.76 ± 0.09
N. Pacific *In-situ*	-13.5 ± 0.4	0.8 ± 0.5	-10.8 ± 0.4	4.7 ± 0.7

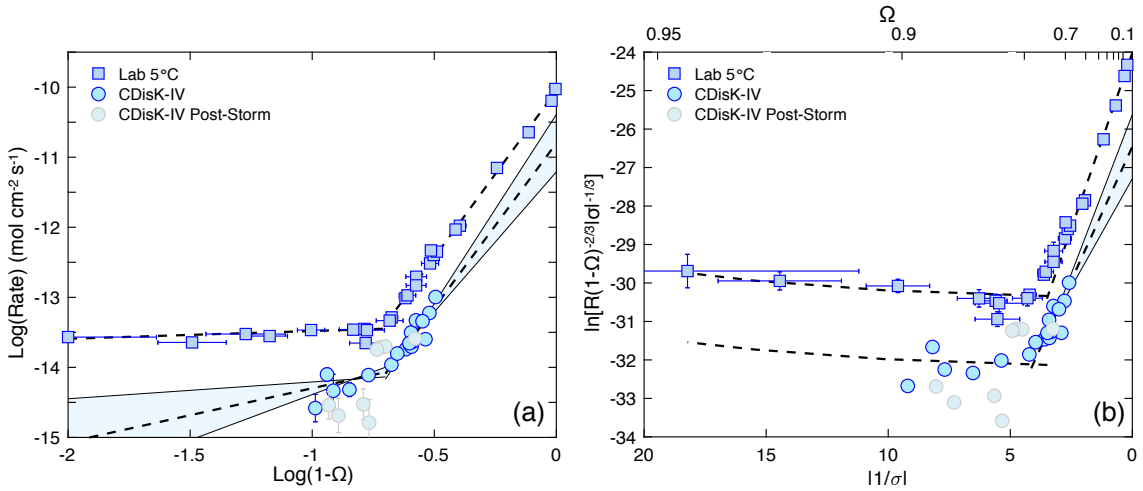

Figure 2.11: (a) Log(Rate) (mol cm^{-2} s^{-1}) versus Log(1-Ω) for our lab and *in-situ* measurements. The fits to the data are from Table 2.2. (b) The normalized dissolution rate (m s^{-1}) versus $\left|\frac{1}{\sigma}\right|$. The x-axis is reversed from Naviaux et al. (2019) to ease comparison with (a). Tick marks are included at intervals of 0.1 Ω units, with one extra tick at Ω=0.95 to emphasize the non-linear nature of the $\left|\frac{1}{\sigma}\right|$ axis. Data from $20>\left|\frac{1}{\sigma}\right|>4.4$ (0.95>Ω>0.8) are fit to Eq. (2b) for dissolution by the retreat of pre-existing steps. Data from $4.4>\left|\frac{1}{\sigma}\right|>0$ (0.8>Ω>0) are fit to Eq. (2a) for dissolution by homogenous etch pit formation. Fitting parameters are in Table 2.3.

The 2D nucleation framework from Dove et al. (2005) allows for the identification of dissolution mechanisms and surface energetics by plotting normalized dissolution rates

versus $\left|\frac{1}{\sigma}\right|$ and fitting to Eq.'s (2a) and (2b) (Dong et al., 2018; Naviaux et al., 2019b; Subhas et al., 2018, 2017) (Figure **2.11**b). The fits to the data and the values for each parameter are available in Table 2.3. Normalized dissolution rates in the lab and *in-situ* are non-linear for $\left|\frac{1}{\sigma}\right| > 4.4$ ($\Omega > 0.8$), consistent with dissolution proceeding from the retreat of pre-existing steps and screw dislocations (Eq. 2b). The *in-situ* data can be fit by Eq. (2b) using the same step edge free energy, α (= -0.5 mJ m^{-2}), as the 5°C lab data, but the *in-situ* data require a step kinetic coefficient, β, that is one order of magnitude lower ($5 \cdot 10^{-8}$ versus $3 \cdot 10^{-7}$ m s^{-1}). Both datasets become linear upon surpassing $\left|\frac{1}{\sigma}\right| \approx 4.4$ ($\Omega = 0.8$), consistent with a mechanistic transition from step retreat to homogenous etch pit formation. The slopes of the data, which are proportional to the step edge free energies, are similar in this far-from-equilibrium region, but the intercepts differ by 2 - 4 natural log units. The intercept of Eq. (2a) is set by both β and the number of active etch pit nucleation sites, n_s, so we make the simplifying assumption that n_s is the same both in the lab and *in-situ* ($5 \cdot 10^{12}$ sites m^{-2}, Naviaux et al., 2019). This assumption is justified because the *in-situ* dissolution rates are slower across each mechanistic regime, and β is the only kinetic variable appearing in both Eq. (2a) and (2b) that affects the magnitude of the rate. Our fits suggest that the components slowing dissolution *in-situ* inhibit the surface retreat rate via β, while minimally affecting the step edge free energies and Ω_{crit}s for the transition between dissolution mechanisms.

Table 2.3: Fits to 2D Nucleation Equations							
Condition	Step Retreat (Eq. 2b) $\left\|\frac{1}{\sigma}\right\| > 4.4$ ($\Omega > 0.8$)			Etch Pit Formation (Eq. 2a) $4.4 > \left\|\frac{1}{\sigma}\right\|$ ($0.8 > \Omega$)			
	$\beta \cdot 10^{-7}$ (m s^{-1})	α (mJ m^{-2})		$\beta \cdot 10^{-3}$ (m s^{-1})	α (mJ m^{-2})		
Laboratory 5°C	3 ± 0.5	-0.5		4.0 ± 0.02	-37.6 ± 0.7		
N. Pacific *In-situ*	0.4 ± 0.2	-0.5		0.35 ± 0.2	-32 ± 3		
Shared Constants							
m[1] (m)	h[2] (m)	a[2] (m)	ω[3] (m^3)	P[4] (m)	K_{sp}'[5] (mol^2 kg^{-2})	C_e[6] (atoms m^{-3})	n_s[1] (sites m^{-3})
1	$3 \cdot 10^{-10}$	$3 \cdot 10^{-10}$	$6.12 \cdot 10^{-29}$	$1.88 \cdot 10^{-9}$	$4.309 \cdot 10^{-7}$	$2.595 \cdot 10^{22}$	$5 \cdot 10^{12}$

[1]Naviaux et al. (2019), [2]Teng (2004), [3]calculated from calcite density of 2.71 g cm^{-3}, [4]estimated assuming burgers vector $b = mh$, $P = 2\pi b$ analogously to Dove et al., 2005, [5]K_{sp}' at 5°C from Mucci (1983), [6]from $K_{sp}'/[Ca^{2+}]$, where $[Ca^{2+}] = 0.01$ M, Naviaux et al (2019)

Dong et al. (2018) documented a pressure dependent enhancement of calcite dissolution rates in the lab, but we are unable to evaluate this effect *in-situ*. The magnitude of the rate enhancement reported by Dong et al. (~2-4x at 700 dbar) is comparable to the scatter of our *in-situ* measurements pre/post-storm. Whereas *in-situ* dissolution rates generally increase with depth (Figure **2.7**), we do not have enough data to identify a change in rate due to Ω, versus a rate enhancement due to pressure. This was a goal of our cruise, but weather and ship problems prevented us from completing this part of the work.

2.4.3 Role of Inhibitors

2.4.3.1 Soluble Reactive Phosphate (SRP)

Our results show that SRP does not inhibit bulk calcite dissolution rates at any of our investigated temperatures or saturation states, even when concentrations exceed modern ocean water column values by an order of magnitude (Figure **2.8**). The idea that SRP is the primary inhibitor in our system is also challenged by our results in archived N. Pacific seawater. The archived seawater had low SRP similar to our laboratory Dickson seawater (0.293 vs. 0.3-0.5 μM), but dissolution rates were slower than in the laboratory water.

SRP is still cited as the canonical calcite dissolution inhibitor (Finneran and Morse, 2009; Morse et al., 2007), but we are not the first to call this into question. Seminal works by Berner and Morse (1974) and Sjöberg (1978) reported SRP inhibiting calcite dissolution rates at concentrations < 10 μM, but later experiments by Walter and Burton (1986) saw no inhibitory effects for SRP < 50 μM. More recently, an atomic force microscopy study by Klasa et al. (2013) documented inhibition for ammonia salts of phosphate, but not for sodium salts typically used in previous studies.

A plausible hypothesis proposed by Walter and Burton (1986) is that dissolution inhibition by SRP is only significant at pHs > 8. The dominant forms of SRP above pH ~ 8 are HPO_4^{2-} and PO_4^{3-}, and seawater precipitation studies have shown that the concentration of PO_4^{3-} ions (Mucci, 1986), and the ratio of PO_4^{3-} to HPO_4^{2-} ions (Burton and Walter, 1990), are better predictors of rate inhibition than the total SRP concentration. The pH-dependence hypothesis may explain why inhibition was reported by Sjöberg (1978, pH = 8.3), but not for this study (pH = 5.5 – 7.5), Walter and Burton (1986, pH = 7.0 – 7.5), or Klasa et al. (2013, pH = 5 and 8), but it cannot explain all results. Though it is possible that the inhibition documented by Berner and Morse (1974, pH 7 – 7.5) was due to pH-probe drift (Walter and Burton, 1986), Alkattan et al. (2002) more recently reported SRP concentrations ≥ 50 μM inhibiting calcite dissolution rates from pH -1 – 3.

We acknowledge that the effects of SRP are complex, and that our results only extend to its role, or lack thereof, in seawater calcite dissolution kinetics. SRP adsorbs to the calcite surface (de Kanel and Morse, 1978; Millero et al., 2001) and has a clear inhibitory effect on calcite precipitation kinetics (Dove and Hochella, 1993). Klasa et al. (2013) did not report any change in the calcite surface retreat rate in undersaturated solutions, but the presence of SRP significantly altered etch pit morphology. Seawater calcite dissolution rates may not be impacted by SRP concentrations ≤ 20 μM from pH 5.5 – 7.5, but it is important to consider the effects of SRP on precipitation rates and surface morphology when studying marine carbonates.

2.4.3.2 Dissolved Organic Carbon

All of our results point to DOC being the primary class of compounds inhibiting calcite dissolution rates in natural seawater. Increased SRP concentrations had no effect on dissolution rates, but the addition of DOC in the form of D-glucose and oxalic acid caused laboratory-derived dissolution rates to slow to comparable values as those observed *in-situ*. This conclusion is further supported by the experiments in archived N. Pacific seawater, in which calcite dissolution rates were initially slow, but matched rates in Dickson seawater after its DIC increased. The archived water was stored in a gas impermeable bag and did not leak, so we propose that the dissolution rate increased due to the quantitative conversion of non-redfieldian organic matter to DIC by respiration. This hypothesis is based on two pieces of evidence: (1) The temporal pattern of the archived water DIC is similar to a biological activity curve. Exponential respiration rapidly consumes available resources, the non-redfieldian nature of which is suggested by the lack of change in alkalinity despite the 152 μmol kg^{-1} change in DIC. No further growth occurs after the limiting resource is exhausted, and the DIC and alkalinity of the archived seawater remained constant for the following 6 months. We speculate that O_2 was the limiting resource, as the DIC increase was comparable to the seawater O_2 concentration before it was transferred to an airtight bag. (2) The chemical addition experiments revealed that DOC can inhibit calcite dissolution kinetics. Organic respiration is a potential mechanism by which an inhibitory organic compound could be converted to a non-inhibitory form in our closed system.

Inhibition by DOC qualitatively explains the internal variability of the shallow and post-storm *in-situ* dissolution measurements. Dissolution reactors deployed below 250 m fell on a consistent rate versus Ω trend, but reactors above 250 m at Station 5 did not (Figure **2.7**). This has parallels to vertical profiles of DOC, where concentrations as high as 80-250 μM in surface waters decrease rapidly to < 50 μM below ~200 - 400 m (Druffel et al., 1992; Hansell, 2013; Hansell and Carlson, 1998a). Furthermore, a phytoplankton bloom was observed after the storm at Station 5, and blooms are known to be associated with dramatic increases in DOC (Eberlein et al., 1985; Hansell and Carlson, 1998b; Ittekkot et al., 1981; Kirchman et

al., 2001)**.** The shallow reactors would have been most susceptible to the variable DOC concentrations after the storm, as well as any potential effects from the phytoplankton bloom.

The conclusion that DOC inhibits calcite dissolution appears to stand in contrast with previous reports (Morse, 1974; Oelkers et al., 2011; Sjöberg, 1978), but, as evident from the fitted *k* values in Table 2.2, dissolution rates in natural seawater are only slower by a factor of ~4 compared to those in poisoned, filtered, UV-treated seawater. It is possible that the ~10% error in Ω and/or rate typical of older studies (Morse, 1974; Sjöberg, 1978) obscured the inhibitory effect of DOC, especially close to equilibrium where rates would have been near the detection limit. For more recent studies (Jordan et al., 2007; O. S. Pokrovsky et al., 2009), the disagreement may simply be due to what the authors deemed "significant" inhibition. For example, Oelkers et al. (2011) measured calcite dissolution kinetics in 0.1M NaCl in the presence of 18 different organic ligands. The authors reported "negligible" ~2.5x rate inhibition by gum xantham, but this decrease is of the same magnitude as the rate offset we document in natural seawater. Finally, biological activity has been shown to enhance DOC adsorption onto calcite (Zullig and Morse, 1988), so it is possible that studies in sterile solutions have underestimated the amount of DOC adsorption, and therefore dissolution inhibition, that occurs in natural environments.

DOC in the ocean is abundant and poorly characterized (Aluwihare et al., 2002; Benner et al., 1992; Hansell, 2013; Hansell and Carlson, 1998b; Repeta et al., 2002), so there are likely a wide range of compounds that can inhibit calcite dissolution kinetics. The inhibitor concentrations in this study were specifically chosen to maximize any potential inhibitory response. Our results therefore only establish that DOC, as a class of compounds, can explain why *in-situ* dissolution rates are slower than in the lab. A study in seawater analogous to that of Oelkers et al. (2011) in dilute solutions will be necessary to further narrow the field of potential dissolution inhibitors.

2.4.4 Implications for *In-situ* Calcite Dissolution Rates

Our data envelope all previous *in-situ* dissolution measurements of inorganic calcite, regardless of depth or location (Figure **2**.**12**). Honjo & Erez (1978) measured the dissolution

rates of crushed calcite in the Sargasso Sea (33°22.0'N, 55°00.8'W) at a depth of 5518 m, and their two overlapping points fall directly upon our 5°C laboratory data. Troy et al. (1997) used AFM to quantify the dissolution rate of Iceland spar calcite moored at Station ALOHA (22°45'N, 158°W) from 350-1000 m. Their rates are more consistent with the slower dissolution rates we measured *in-situ*. Peterson (1966) measured the mass loss of moored calcite spheres in the Central Pacific (18°49'N, 168°0.31'W) after 4 months. Saturation data were not reported by Peterson, so we plot his points against $\Omega_{(Alk,\ pH)}$ measured on the 2015-P16 cruise at the same latitude (18°49'N, 152°W). When doing so, Peterson's rates span the range between our lab and *in-situ* measurements and reveal a reaction rate kink at the same Ω_{crit}. The P16 $\Omega_{(Alk,\ pH)}$ is used, rather than the $\Omega_{(Alk,\ DIC)}$ at the location of Peterson's experiments from Takahashi (1975), due to the discrepancy in the Ω calculations that was discussed in Section 2.3.1. The difference is small, but plotting against the Takahashi Ω shifts the data ~0.02 units closer to equilibrium (Figure **2**.**13**). We note that the Takahashi Ω value implies that the dissolution measured by Peterson from 500-2000 m occurred in supersaturated waters, whereas $\Omega_{(Alk,pH)}$ does not. Finally, Fukuhara et al. (2008) moored crushed calcite in the Central Pacific (29°59.95'N, 175°00.17'E) from 1668-5167 m. The data are not included in Figure **2**.**12**, as the authors did not report the surface area of their material. Nevertheless, the rates are similar to our own (order of $\sim 1 \cdot 10^{-14}$ mol cm^{-2} s^{-1}) if we assume the same surface area as that measured by Honjo & Erez for crushed calcite (0.35 m^2 g^{-1}).

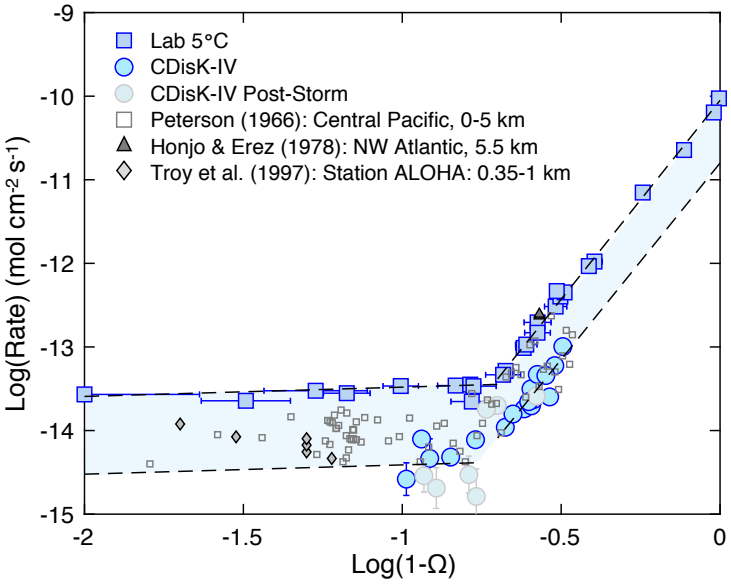

Figure 2.12: Compilation of *in-situ* dissolution rates of inorganic calcite overlaid upon our measured lab and *in-situ* rates. The rate data from Honjo & Erez (1978) are from their Table 2 for reagent calcite and large calcite crystals, and Ω is from Takahashi (1975). Rate and Ω data for Troy et al. (1997) are from their Figure 12. Troy et al. documented dissolution above the saturation horizon, but these data are not included. Peterson (1966) rate data are from Fig. 2 of his paper, with Ω from 2015-P16 at a comparable location (see text for details, as well as Fig. S5). The shaded area represents theoretical bounds for dissolution in low DOC (top curve) and high DOC (bottom curve) seawater. The bounds are fit by the 5°C *n* and *k* values in Table 1. The lower bound is fit by $R=10^{-14.3\pm0.2}(1-\Omega)^{0.11\pm0.1}$ for $0.8 < \Omega < 1$, and $R=10^{-10.8\pm0.4}(1-\Omega)^{4.7\pm0.7}$ for $0 < \Omega < 0.8$.

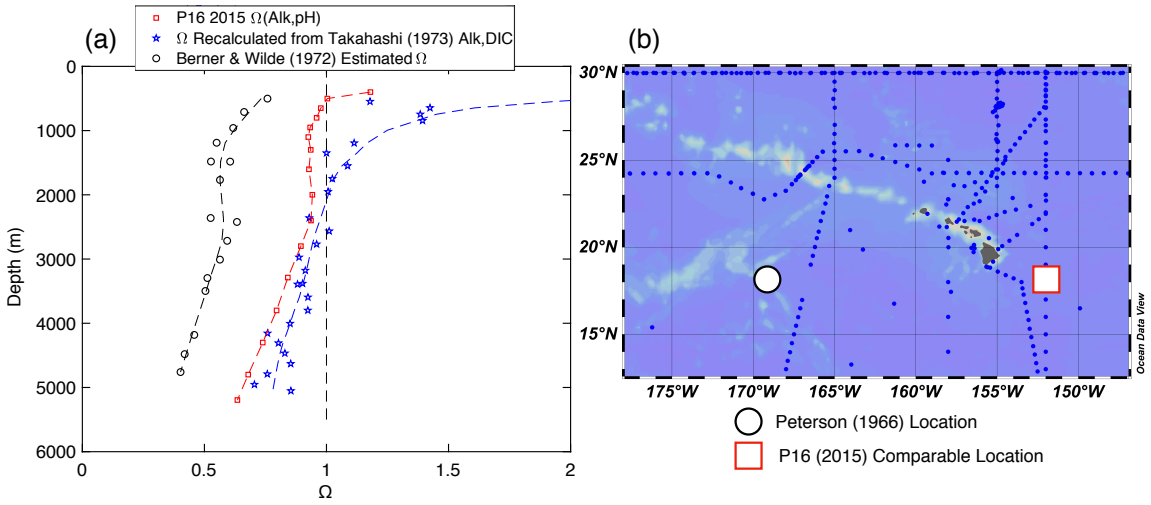

Figure 2.13: (a) Estimates for the saturation state at the location of Peterson's (1966) moored calcite spheres. Ω estimates by Berner & Wilde (1972) are from their Table 2 and were based upon measurements of pH and carbonate alkalinity near Peterson's deployment site. Takahashi subsequently returned to the Peterson deployment site in 1973 and measured the total alkalinity, DIC, salinity, and temperature. The Takahashi data was taken from GLODAP v2 Bottle Data (Station ID: 33541, EXPOCODE: 318M19730822) and input into CO2SYS using the carbonate system parameters outlined in the main text. The resulting $\Omega_{(Alk, DIC)}$ is similar to the ΔpH profile in Fig. 8 published by Takahashi (1975), but our calculated Ω has a shallower slope versus depth. The profiles match to a depth of 3000 m, but we calculate Ω=0.7 at 5000 m compared with Takahashi Ω = 0.4 (ΔpH = 0.2, Fig. 8 of their paper). Given the issues with $\Omega_{(Alk, DIC)}$ discussed in the text, Peterson's data were plotted versus $\Omega_{(Alk, pH)}$ measured at the same latitude on a 2015 P16 cruise. (b) The P16 line was 20° East of the Peterson site, but the profile is similar in shape to the original Berner & Wilde estimate. Peterson documented dissolution from 500-2000 m, and these depths are undersaturated by P16 $\Omega_{(Alk, pH)}$, but supersaturated for Takahashi $\Omega_{(Alk, DIC)}$.

The heterogeneity of the nature and concentrations of DOC in the ocean implies that calcite dissolution rates possess an innate degree of variability. In fact, some of this variability was documented in our post-storm data. Given our understanding of DOC as a source of rate variance, our lab and *in-situ* data may be considered end member cases for dissolution rates in low/high DOC waters, and can help explain differences among previous *in-situ* rate measurements. Studies producing relatively slow dissolution rates used calcite material that was exposed to high DOC surface seawater as it was lowered through the water column (Peterson, 1966; Troy et al., 1997; Fukuhara et al., 2008) and may be described by the *in-situ*

parameters in Table 2.2. The historical data compilation supports the use of a small reaction order for $0.8 < \Omega < 1$, so we fit the lower bound using the same n as our laboratory data, such that $R_{(mol\ cm\text{-}2\ s\text{-}1)} = 10^{-14.3\pm0.2}(1\text{-}\Omega)^{0.11\pm0.1}$ for $0.8 < \Omega < 1$. The Dickson seawater used in the lab was filtered, poisoned, and UV treated, and represents the upper bound for dissolution rates in low DOC waters. This upper bound is fit by the laboratory n and k values in Table 2.2. Honjo and Erez (1978) present a useful *in-situ* example of this upper bound, as the authors prevented their material from contacting ambient seawater until reaching the desired depth. Their crushed calcite was exposed only to low DOC abyssal waters, and the rate that they recovered matched the upper limit of our lab measurements. For the purposes of modeling water column calcite dissolution, we recommend that the lower bound be used, as natural carbonates form in high DOC surface waters and dissolve as they sink.

2.5 Conclusion

We dissolved ^{13}C-labeled inorganic calcite both in the lab and *in-situ* across a transect of the N. Pacific. We find that $\Omega_{(alk,\ pH)}$ provides a better description of marine carbonate chemistry than $\Omega_{(alk,DIC)}$, and in doing so, we echo the need for a thorough reevaluation of pK_1', pK_2', and the total boron-salinity ratio (Fong and Dickson, 2019). When uncorrected, the use of $\Omega_{(alk,DIC)}$ can shift down the $\Omega = 1$ saturation horizon by ~5-10%. Caution should therefore be used when calibrating proxies to GLODAP $\Omega_{(alk,DIC)}$ water chemistry. Calcite dissolution rates exhibited the same dependence on undersaturation in the lab and *in-situ*, with fits to the empirical $Rate = k(1\text{-}\Omega)^n$ equation yielding reaction orders of $n < 1$ for $0.8 < \Omega < 1$, and $n = 4.7$ for $0 < \Omega < 0.8$. The change in the reaction order at 5°C at $\Omega_{crit} = 0.8$ is consistent with a change in dissolution mechanism from step retreat to homogenous etch pit formation. *In-situ* dissolution rates were slower than those in the lab by a factor of ~4 due to the presence of natural inhibitors. Chemical spike experiments revealed that soluble reactive phosphate had no effect on calcite dissolution kinetics under our experimental conditions, but the addition of DOC in the form of oxalic acid and D-glucose slowed dissolution to match *in-situ* observations. DOC appears to act by inhibiting the rate of retreat of the calcite surface. Our lab and *in-situ* rate data form an envelope around previous *in-situ* dissolution measurements and may be considered outer bounds for dissolution rates in low/high DOC waters. The lower

bound is most realistic for particles sinking out of surface waters and should be used for modeling water column calcite dissolution rates. It may be fit by $R_{(mol\ cm\text{-}2\ s\text{-}1)} = 10^{-14.3\pm0.2}(1-\Omega)^{0.11\pm0.1}$ for $0.8 < \Omega < 1$, and $R_{(mol\ cm\text{-}2\ s\text{-}1)} = 10^{-10.8\pm0.4}\ (1-\Omega)^{4.7\pm0.7}$ for $0 < \Omega < 0.8$.